Spatial single-cell isotope tracing reveals heterogeneity of *de novo* fatty acid synthesis in cancer cells

Elena Buglakova[1], Marteinn Snaebjornsson[2], Maans Ekeloef[1], Lisa Schlicker[2], Martijn R. Molenaar[1], Shahraz Mohammed[1], Lachlan Stuart[1], Andreas Eisenbarth[1], Volker Hilsenstein[1], Almut Schulze[2,+], Theodore Alexandrov[1,3,4,+]

1 Structural and Computational Biology Unit, European Molecular Biology Laboratory (EMBL), Heidelberg, Germany
2 German Cancer Research Center, Division of Tumor Metabolism and Microenvironment, Im Neuenheimer Feld 581, 69120 Heidelberg, Germany
3 Metabolomics Core Facility, EMBL, Heidelberg, Germany
4 BioStudio, BioInnovation Institute, Copenhagen, Denmark

+ corresponding authors

Email: theodore.alexandrov@embl.de, almut.schulze@dkfz-heidelberg.de

Keywords: spatial single-cell metabolomics, stable isotope tracing, single-cell analysis, fatty acid synthesis, acetyl-CoA production, ACLY, cancer

Abstract

Metabolism has emerged as a key factor in homeostasis and disease including cancer. Yet, little is known about the heterogeneity of metabolic activity of cancer cells due to the lack of tools to directly probe it. Here, we present a novel method, ^{13}C-SpaceM for spatial single-cell isotope tracing of glucose-dependent *de novo* lipogenesis. The method combines imaging mass spectrometry for spatially-resolved detection of $^{13}C_6$-glucose-derived ^{13}C label incorporated into fatty acids composing cellular lipids with microscopy and computational methods for data integration and analysis. We validated ^{13}C-SpaceM on a spatially-heterogeneous normoxia-hypoxia model of liver cancer cells. We demonstrated the single-cell heterogeneity of acetyl-CoA pool labelling degree upon ACLY knockdown that is hidden in the bulk analysis and its effect on synthesis of individual fatty acids. Overall, ^{13}C-SpaceM provides a capacity to probe metabolic activity on the single-cell level.

Introduction

Lipids are a highly complex class of hydrophobic biomolecules that are involved in multiple cellular functions. For example, glycerophospholipids and sphingolipids are major structural components of cellular membranes [1] while triglycerides stored in lipid droplets provide cells with an additional energy source [2]. Lipids can also contribute to cellular signaling pathways by functioning as second messengers or lipid mediators [3-5]. Altered lipid metabolism is a hallmark of many cancers, as it is a prerequisite for rapid growth and proliferation and promotes survival under nutrient limiting conditions [6-8]. Altered lipid metabolism in cancer also contributes to oxidative stress resistance and activates oncogenic signaling pathways through the production of lipid mediators [9]. Lipid metabolism is also affected by different stresses imposed by the tumor microenvironment, such as limited nutrient and oxygen supply [10]. Therefore, cancer cells need to adapt to these stresses by adopting different routes for the provision of lipids, thus inducing selective metabolic dependencies that could be targeted for cancer therapy.

Most lipids are synthesized from fatty acids, a group of small linear molecules consisting of a carboxylic acid head and an aliphatic tail (Fig. 1a). Fatty acids differ in their length and degree of saturation, i.e. the number of double bonds located in different positions of the hydrocarbon chain [11]. Cells in the adult mammalian organism generally take up fatty

acids from the blood stream. However, cells of adipose and hepatic tissues as well as various cancers can also generate fatty acids through *de novo* synthesis using acetyl-coenzyme A (acetyl-CoA) as a substrate [7]. The first step in fatty acid biosynthesis consists of the conversion of acetyl-CoA into malonyl-CoA by acetyl-CoA synthetases (ACC1/2). Malonyl-CoA is then used by fatty acid synthase (FASN), a large enzyme with multiple catalytic centers, for the repeated condensation reactions of two-carbon units, derived from acetyl-CoA, to form palmitate (16:0), a 16-carbon saturated fatty acid. Palmitate can then be further elongated and/or desaturated thus generating a variety of saturated and monounsaturated fatty acids that can subsequently be incorporated into the lipidome. The fatty acid composition (or saturation state) of the lipidome is a critical factor for cell survival under metabolically challenging conditions. An example of this is the mono-unsaturated fatty acid oleate which protects cancer cells from lipotoxicity and ER stress [12-15], inhibits apoptosis [16] and promotes ferroptosis resistance [17]. Indeed, is has been shown that hypoxic and Ras-transformed cells preferentially take up mono-unsaturated fatty acid to support proliferation and survival [18].

The cytoplasmic (lipogenic) acetyl-CoA pool used as a substrate for fatty acid synthesis can be derived from different precursors through specific metabolic routes. Glucose-derived carbons provide fuel for the production of citrate by the TCA cycle in the mitochondrial matrix. This citrate is then exported from the mitochondria and used in the cytoplasm by ATP citrate lyase (ACLY) to generate acetyl-CoA. However, the use of glucose as a precursor for fatty acid synthesis is limited under certain conditions, such as hypoxia, in which glucose-derived pyruvate is diverted away from mitochondrial metabolism and converted to lactate. Under these conditions, glutamine can substitute as a precursor for fatty acid synthesis through the reductive carboxylation of glutamate to citrate [19, 20]. Furthermore, hypoxic cancer cells also use acetate as a precursor for fatty acid biosynthesis through acetyl-CoA synthetase 2 (ACSS2) [21, 22].

Besides its function as a substrate for fatty acid synthesis, acetyl-CoA is also needed for the post-translational modification of proteins, most importantly histones for chromatin regulation [23]. Indeed, both ACLY and ACSS2 have been found to localize to nucleus and

modulate histone acetylation and thus affect gene expression [24, 25]. The modulation of acetyl-CoA metabolism by oncogenic signaling pathways and environmental factors can thereby affect complex gene expression programs in cancer cells. Monitoring the interplay between fatty acid synthesis and acetyl-CoA metabolism therefore provides vital information on the state of cancer cells.

The advent of single-cell tools has revolutionized the analysis of individual cells within heterogenic populations [26]. While metabolomics provides much more dynamic information about cellular states, its application at single-cell level has somewhat lagged behind single-cell transcriptomic and proteomic techniques, due to the immense technical challenges [27]. The high metabolic heterogeneity of cancer cells makes it essential to develop analysis tools that are capable of interrogating fatty acid synthesis and acetyl-CoA metabolism in cancer cells on the single-cell level. Different experimental methods have been applied to evaluate the heterogeneity of lipid metabolism in cancer cells. For example, a metabolic sensor based on the malonyl-CoA responsive Bacillus subtilis transcriptional repressor, FapR, was developed to determine the activity of FASN in live cells [28]. Another approach used surface-immobilized dendrimers to evaluate fatty acid uptake on a single cell level [29]. Furthermore, a recent study applied dielectric barrier discharge ionization (DBDI) on single cells to determine alterations in lipid metabolism upon ACLY inhibition in pancreatic cancer cells [30]. However, these methods fail to provide information about metabolic precursors of fatty acid synthesis and do not afford sufficient molecular resolution to interrogate acetyl-CoA metabolism.

We previously developed a spatially resolved mass-spectrometry pipeline for the quantification of intracellular metabolites at single-cell resolution [31]. Stable-isotope tracing has been used to determine *de novo* fatty acid biosynthesis and the contribution of different metabolic precursors to the cytoplasmic acetyl-CoA pool [21, 32]. We now describe ^{13}C-SpaceM, a method that combines stable isotope tracing with the detection of fatty acids present as acyl-chains in selected lipid classes in a spatially resolved manner, using MALDI-MS2. We applied this method to interrogate the effect of hypoxia on *de novo* fatty acid synthesis in a population of murine liver cancer cells. Moreover, we also developed

a method to evaluate the effect of genetic depletion of ACLY on the contribution of glucose to the cytoplasmic acetyl-CoA pool on a single cell level. Our results show that ^{13}C-SpaceM can reveal substantial heterogeneity in fatty acid synthesis and acetyl-CoA metabolism in cancer.

Material and Methods

Cell culture for the normoxia-hypoxia model

Primary murine liver cancer cells derived from a Myc- and Akt-driven tumor model (*Myc*^{OE}; *Akt*^{Myr}; *Tp53*$^{-/-}$) [15] were a gift from Daniel Dauch (University of Tübingen). Cells were cultured in DMEM supplemented with 1 mM acetate, 2 mM glutamine and 10% FCS in a 37°C incubator with 5% CO_2 either under normoxia (20% O_2) or hypoxia (0.5% O_2) in the presence of $^{13}C_6$-glucose for 72 hours. Hypoxic conditions (0.5% O_2) were induced in a hypoxia workstation (H35, Don Whitley). The cells cultured under hypoxic conditions were modified to express Green Fluorescent Protein (GFP) as a marker. For ^{13}C-SpaceM, the normoxic and hypoxic cells were mixed using 10,000 cells of each condition, plated on the same glass slide and allowed to attach for 3 hours before fixation.

ACLY knockdown

For the ACLY knockdown, we used the same primary murine liver cancer cells as in the hypoxia model. shRNA sequences targeting murine Acly or non-targeting controls were cloned into LT3-GEPIR (Addgene), the shRNA sequences used were (TGCTGTTGACAGTGAGCGACCGCAGCAAAGATGTTCAGTATAGTGAAGCCACAGATGTATACTGAACATCTTTGCTGCGGCTGCCTACTGCCTCGGA), (TGCTGTTGACAGTGAGCGAACCAGTGTCTACTTATGTCAATAGTGAAGCCACAGATGTATTGACATAAGTAGACACTGGTCTGCCTACTGCCTCGGA), (TGCTGTTGACAGTGAGCGCAGGAATTATAATGCTTATCTATAGTGAAGCCACAGATGTATAGATAAGCATTATAATTCCTATGCCTACTGCCTCGGA) for ACLYkd oligo 1, oligo 2 and nontargeting control, respectively. Lentiviral particles were produced in HEK293 cells after transient transfection of the packaging vectors psPAX.2 and pMD.G2 (Addgene #12260 and #12259). After viral transduction, liver cancer cells were selected with puromycin and used at low passage. Induction of shRNA expression was achieved by treating cells with 1µg/ml doxycycline (Sigma) for 72 hours. For stable isotope tracing, cells were cultured in glucose-free DMEM supplemented with $U^{13}C_6$-

glucose (Cambridge Isotope laboratory, Tewksbury, Massachusetts) and 1mM acetate for 72hrs.

Liquid-chromatography coupled with mass spectrometry (LC-MS)

For bulk LC-MS, cells were washed with cold 154 mM ammonium acetate, snap frozen in liquid nitrogen and harvested in methanol/H_2O (80/20, v/v) with added standards (10 µL of 100 µM Palmitate-2,2-D2 (Eurisotop: DLM-1153-0)/ 1 x 10E6 cells). 30 µL 0.2 M HCl, 2 x 100 µL $CHCl_3$, 2 x 100 µL H_2O was then added with vortexing in between. The suspension was centrifuged at 16,000 g for 5 min, the lower lipid phase was then washed with synthetic polar phase (CH_3Cl/Methanol/H_2O, 58/33/8, v/v/v) and evaporated to dryness under N_2 at +45°C. For saponification, lipids were resuspended in Methanol/H_2O (80/20, v/v) containing 0.3 M KOH, heated at +80°C for 1 h and washed twice with 0.5 mL hexane. After addition of 50 µL formic acid, fatty acids were subsequently extracted twice with 0.5 mL hexane and evaporated to dryness under N_2 at +45°C. For LC/MS analysis the fatty acids, were dissolved in 100 µL isopropanol and 5 µL of each sample was applied to a C8 column (Acclaim RSLC C8 column, 2.2 µm particles, 50 × 2.1 mm, Thermo Fisher Scientific) at +40°C, with mobile phase buffer A consisting of 0.1% formic acid in CH_3CN/H_2O (10/90, v/v), and solvent B consisting of 0.1% formic acid in CH_3CN/H_2O (90/10, v/v). The flow rate was maintained at 350 µL/min and eluent was directed to the ESI source of the QE-MS from 3 min to 27 min after sample injection. MS analysis was performed on a Q Exactive Plus Orbitrap mass spectrometer (Thermo Fisher Scientific) applying the following settings: Sheath gas, 30; spray voltage, 2.6 kV. Capillary temperature +320°C, aux gas heater temperature: +120°C and S-lens voltage was 55. A full scan range from 150 to 460 (m/z) in negative ion mode was used. The resolution was set at 70,000. The maximum injection time was 100 ms with an AGC-target of 1E6 ions. Peaks corresponding to the calculated fatty acid masses (±5 ppm) were integrated using El-Maven (https://resources.elucidata.io/elmaven) and correction for natural ^{13}C isotopic abundance was done using IsoCorrectoR [33].

SpaceM Analysis

The SpaceM [31] method for fusion of microscopy and MALDI-MS spatial metabolomics data was applied to analyze the de-novo synthesis of fatty acids on a single-cell level.

Microscopy

After cell culturing, the cells were washed with PBS, fixed using Histofix (Roth, 87.3) for 10 minutes, stained using DAPI, washed 3x in PBS and then desiccated in a Lab Companion Cabinet Vacuum Desiccator for 30 min at room temperature and −0.08 MPa. Pre-MALDI brightfield and fluorescent microscopy (620 and 460 nm) images were obtained with a DS-Qi2 camera (Nikon Instruments) with a Plan Fluor 10x (numerical aperture (NA) of 0.30) objective (Nikon Instruments) mounted on a Ti-E inverted microscope (Nikon Instruments). The pixel size was 0.64 µm. For the hypoxia experiment, additional pre-desiccation microscopy images were collected. Rigid registration of pre-desiccation and post-desiccation microscopy images was performed using the Affinder plugin in Napari (https://www.napari-hub.org/plugins/affinder). The cells were imaged in bright-field microscopy after MALDI-imaging, using the same microscopy setup and parameters.

Microscopy image analysis

Cells in the bright-field channel of pre-MALDI microscopy were segmented using a custom Cellpose model [34] trained on manually annotated fragments of images. Since the primary cell culture contains cells of varying size, segmentation for the largest cells had to be manually corrected. Ablation marks were detected in the post- MALDI microscopy by manually fitting a grid of circular shapes. Registration of the pre- and post-MALDI images was done using the SpaceM software tool as previously published [31].

MALDI imaging

The MALDI matrix 1,5-diaminonaphthalene (DAN) was applied to a surface density of 3 µg/µm^2 immediately before MALDI analysis using a TM sprayer (HTX Technologies, Chapel Hill, NC, USA). Atmospheric pressure MALDI imaging was performed using an AP-SMALDI5 ion source (TransMIT GmbH, Gießen, Germany) coupled to a Q Exactive Plus Orbitrap mass spectrometer (Thermo Fisher Scientific). For all experiments the

raster pitch was 10x10 µm, with the laser attenuator angle set to 33°. The mass spectrometer method used was set up as all-ion fragmentation (AIF) in negative ion mode, with an isolation range of 600-1000 and a scan range of 100-400 at 140,000 nominal resolving power with 500 ms ion injection time. Fragmentation was performed using higher-energy collisional dissociation (HCD) at a normalized collision energy of 25.

Constructing single-cell isotopologue profiles

MALDI images for unlabeled samples were annotated with the cloud software METASPACE (http://metaspace2020.eu) at 5% FDR to determine the most abundant detected fatty acids. For each fatty acid, intensities corresponding to theoretical isotopologue peak masses were extracted. Raw intensities were normalized for natural isotope abundance using IsoCor [35], after which every isotopologue distribution was normalized by its sum. Ablation marks with a total raw intensity of less than 200 for a given fatty acid were removed from the analysis. Ablation marks which had at least 30% overlap with the cell mask were considered intracellular. After normalizing spectra in each pixel, the median of values in the intracellular ablation marks was assigned as a single-cell readout for each isotopologue peak. The resulting single-cell isotopologue distribution for every fatty acid was normalized by its sum again. Scanpy v.1.8.1 [36] was used for all single-cell data analysis.

Calculation of single-cell features

For each well of a multi-well slide, the median intensity of the GFP channel outside of the cell masks was subtracted from the image, and the logarithm of the maximum GFP intensity inside the cell mask was used to characterize single-cell GFP signal. Both in normoxia/hypoxia and in ACLYkd experiments, the 95th percentile of the GFP signal in the GFP-negative wells was used as a threshold to assign cells to either GFP-positive or GFP-negative state.

In addition to the normalized isotopologue peak intensities, a binomial model for the fatty acid synthesis described in [32] was used. Fatty acids are synthesized by randomly taking 2-carbon monomers from the cytosolic AcCoA pool. Therefore, if the fraction of labeled monomers equals *p*, the probability that a given fatty acid has 2i labeled carbons, can be described with the following model:

$$P_{binom}(k) = \binom{n}{k} p^k (1-p)^{n-k}, k = 0,1, \dots n$$
$$I_0 = uptake + (1 - uptake) * P_{binom}(0)$$
$$I_i = (1 - uptake) * P_{binom}(i), i = 1,2, \dots n$$

where uptake is the fraction of the unlabeled FA directly taken from the media, *p* is the labeling degree of cytosolic AcCoA pool, and n is the number of AcCoA molecules used for the synthesis (number of carbons in the fatty acid / 2). Longer fatty acids can be synthesized both using labeled palmitate made by the cell *de novo* and unlabeled palmitate, therefore we used a modified model for C18:

$$I_0 = uptake + (1 - uptake) * P_{binom}(0)$$
$$I_1 = (1 - uptake) * \left(uptake_{C16} + (1 - uptake_{C16}) * P_{binom}(1)\right)$$
$$I_i = (1 - uptake) * (1 - uptake_{C16}) * P_{binom}(i), i = 2,3, \dots n$$

where $uptake_{C16}$ is the fraction of palmitate taken from the medium.

Fitting a binomial model to the single-cell isotopologue distributions allows summarizing them as two numbers: uptake, which characterizes the fraction of the fatty acid which was not synthesized *de novo* but directly taken from the medium, and AcCoA pool labeling degree *p*, which describes relative contribution of the labeled substrate to the fatty acid synthesis compared to other carbon substrates consumed by the cell. The limitation of this method is that if overall substrate usage is very low, such as in the hypoxia/normoxia experiment, it becomes impossible to reliably fit a binomial distribution and estimate the uptake fraction, therefore it was only used for the ACLYkd experiment data analysis.

Results

^{13}C-SpaceM, a method for single-cell isotope tracing

The key development presented in this paper is ^{13}C-SpaceM, a method for single-cell isotope tracing. ^{13}C-SpaceM builds upon SpaceM, a method for single-cell metabolomics which integrates imaging mass spectrometry (imaging MS) for the detection of stable isotope-labeled metabolites and lipids, and microscopy for assigning imaging MS pixels to individual cells and for quantifying fluorescence and morphometric properties of single cells [31]. In contrast to the conventional SpaceM method using MS1, in ^{13}C-SpaceM we exploited a particular type of mass spectrometry, namely Higher-Energy Collision-induced Dissociation All Ion Fragmentation (HCD AIF), where lipids in the range of 600-1000 m/z in the negative mode were simultaneously fragmented and then the fragments in the range of 200-400 m/z were detected (**Fig. 1b**). This allowed us to interrogate fatty acid composition of the cellular lipids. The selected mass range includes most glycerophospholipids (PC, PE, PS, PG, PA, PI), sphingolipids (SM, Cer, HexCer, CerP), neutral lipids such as but does not include smaller lipids such as lysophospholipids or monoradylglycerolipids nor larger lipids such as triglycerides, cardiolipins or PIP-trisphosphates [37]. The exploited negative ion polarity favors detection of phospholipids and sphingolipids. The construction of single-cell profiles was done as in the conventional SpaceM (**Fig. 1c**); see Methods for details.

Spatially-heterogeneous normoxia-hypoxia model for evaluating single-cell isotope tracing

In this work, we focused on applying 13C-SpaceM to interrogate lipid biogenesis through *de novo* fatty acid synthesis, a highly dynamic metabolic process that integrates multiple substrates and contributes to the complexity of cellular lipids (**Fig. 1a**). In order to validate ^{13}C-SpaceM in this context, we developed a controlled spatially-heterogeneous model containing co-plated cells of two distinct phenotypes: cells cultured under either normoxic or hypoxic conditions. We chose this model as hypoxia causes global reprogramming of cellular metabolism, including lipid metabolism. Specifically, hypoxic cells undergo a switch in the use of substrates for the production of cytoplasmic acetyl-CoA used by fatty

acid synthesis, by promoting the reductive carboxylation of glutamine to form citrate [19, 20, 38] or by the direct use of acetate [22]. Moreover, hypoxia blocks fatty acid degradation and induces fatty acid uptake and lipid storage [39]. We therefore anticipated that cells cultured under hypoxia should show decreased incorporation of glucose-derived stable-isotope-labeled carbon atoms into cellular lipids compared to cells cultured under normoxic conditions. As fatty acid synthesis utilizes the cytoplasmic acetyl-CoA pool, analysis of the isotopologues distribution of fatty acids incorporated into cellular lipids allows the assessment of changes in the relative contribution of different substrates to the synthesis of cytoplasmic acetyl-CoA [21]. The workflow employed by ^{13}C-Space allows the quantification of all isotopologues detected for fatty acids released from total cell lipids isolated at a mass range of m/z 600-1000 in the negative mode using all-ion fragmentation (**Fig. 1b**). Registration of pre- and post-MALDI microscopic images to the MALDI-imaging spectra allows the assignment of ion intensities to individual cells (**Fig. 1c**).

^{13}C-SpaceM provides isotopologues profiles for single cells, integrated with microscopy

Pre-MALDI microscopy images overlaying the brightfield and GFP channels for the co-plated normoxic (GFP-negative) and hypoxic (GFP-positive) cells demonstrate a high degree of spatial heterogeneity of these two conditions (**Fig. 2a, first plot**). Cell segmentation and quantification of cellular GFP provides single-cell fluorescence intensities (**Fig. 2a**, **second plot**). The single-cell isotopologues profiles can be constructed by ^{13}C-SpaceM for individual fatty acids incorporated into cellular lipids, for example for palmitate, which is the key intermediate metabolite of the *de novo* fatty acid synthesis. An important parameter which can be calculated based on an isotopologues profile is the fraction of the unlabeled fatty acid, namely the fraction of M+0 compared to other isotopologues. A high fraction of unlabeled palmitate corresponds to low *de novo* fatty synthesis and lipid biogenesis from glucose. Figure 2a (third and fourth plots) illustrate the fraction of unlabeled palmitate as measured by imaging MS in pixelated manner and as calculated for single cells using ^{13}C-SpaceM.

Figure 2b shows the underlying mass spectra collected at two representative pixels, one corresponding to a cell cultured under normoxia (spectral intensities shown in grey, cell outline shown in white) and another corresponding to a cell cultured under hypoxia (spectral intensities and cell outline shown in green); the intensities for the latter are shown in the negative scale for better visualization. For each spectrum, the highest peak corresponds to the unlabeled palmitate (M+0), with additional peaks for higher isotopologues e.g. M+2, M+4, M+6 are marked by circles. The peaks not marked by circles are unrelated to palmitate isotopologues based on the accurate m/z matching within ±3 ppm. Notably, most palmitate isotopologues are present only in the spectrum of the pixel derived from a normoxic cell. The mass spectrum from the hypoxic cell shows an increased peak for the M+0 mass and only two minor additional isotopologues (M+2 and M+10).

^{13}C-SpaceM reveals reduced *de novo* fatty acid synthesis under hypoxia

Before we applied ^{13}C-SpaceM to the spatially-heterogeneous mix of normoxic and hypoxic cells, we interrogated each condition separately. This was performed to validate that the GFP readout is informative of the condition (GFP+ for hypoxia vs GFP- for normoxia) and to evaluate whether isotopologue distribution at the single-cell level can reveal reduced glucose contribution to *de novo* fatty acid synthesis and lipid biogenesis under hypoxia.

Figure 2c shows a single-cell scatterplot showing for each cell its log(GFP intensity) which is the ground-truth readout characteristic of normoxia (x axis) vs unlabeled palmitate fraction calculated using the single-cell isotopologue profiles as the normalized palmitate M+0 intensity (y axis). Palmitate was chosen for this analysis as it is the immediate product of *de novo* fatty acid synthesis by the enzyme fatty acid synthase (FASN) and is readily incorporated into cellular lipids, thus representing the most direct readout of the pathway [7]. Fig. 2c shows that the fractions of unlabeled palmitate are clearly different between normoxic and hypoxic cells plated separately. Cells cultured under hypoxic conditions (shown in green) show normalized M+0 intensities close to 0.9, indicating that only a small amount of palmitate was synthesized from glucose. This

reflects either an overall low rate of *de novo* fatty acid synthesis or a switch from glucose to other substrates, such as glutamine or acetate [21]. This is opposite to cells cultured under normoxia, where the proportion of unlabeled palmitate is substantially lower, indicating higher contribution from ^{13}C-glucose to palmitate synthesis.

Interestingly, cells cultured under normoxia demonstrate a higher heterogeneity (broad distribution of normalized M+0 intensities ranging from 0.4 to 0.8) compared to the cells cultured under hypoxia (narrow distribution of normalized M+0 intensities ranging from 0.85 to 0.95). One explanation for this increased heterogeneity could be that cells cultured under normoxic conditions are more proliferative. Indeed, proliferating cells switch from fatty acid synthesis to fatty acid uptake during different phases of the cell cycle [40]. Nevertheless, despite this higher heterogeneity, cells cultured under normoxia displayed ratios of unlabeled palmitate (< 0.8) that were clearly distinct from those of hypoxic cells (> 0.85). This demonstrates that *de novo* fatty acid synthesis is active in all normoxic cells, with a detectable contribution from glucose to the cytoplasmic lipogenic acetyl-CoA pool.

^{13}C-SpaceM discerns co-plated single normoxic and hypoxic cells

We next examined glucose-dependent palmitate labeling at the single-cell level of cells cultured under normoxia and hypoxia using the spatially-heterogeneous co-plated model, using GFP as the ground-truth for assigning each cell to either normoxia (GFP-) or hypoxia (GFP+) culturing conditions. Cells with log10 GFP intensity of larger than 3 were considered to be from the hypoxia condition. These cells showed a large fraction of unlabeled palmitate (normalized M+0 intensity around 0.9, **Fig. 2d**), indicating low rates of *de novo* fatty acid synthesis form glucose. However, cells identified as low GFP (log10 GFP intensity less than 3) displayed a mixed phenotype with some cells showing a large fraction of unlabeled palmitate (normalized M+0 intensity >0.8) while others showed evidence for palmitate labelling from glucose (normalized M+0 intensity between 0.4-0.8) (**Fig. 2d**). This can also be seen in the mono-plated scenario (**Fig. 2c**) and is most likely caused by a proportion of the hypoxic cells having low levels of GFP expression, potentially due to silencing of the promoter in the expression construct.

Overall, we observed a strong similarity in the values measured for the unlabeled palmitate pool in the mono-plated and co-plated scenarios (**Fig. 2c** cf. **Fig. 2d**). Despite this similarity, the separation of the two cell populations based on unlabeled palmitate was less obvious in the co-plated scenario, as a small proportion of cells show intermediate levels of palmitate labelling (normalized M+0 intensities between 0.75-0.88). This potentially indicates an error of estimating the unlabeled palmitate ratio for the hypoxic cells due to co-sampling of neighboring normoxic cells, and the nature of this error (slight increase of intensities of isotopic peaks at M+1 to M+16, thus reducing the ratio of unlabeled palmitate). However, the presence of two distinct clusters (i.e. cells with high levels of M+0 palmitate vs cells with low levels of M+0 palmitate) and the high similarity between the separate and co-plated cells indicates that the effect of this error is small and still allows a clear separation between the two phenotypes.

We therefore quantified the capacity of ^{13}C-SpaceM and specifically of the ratio of unlabeled palmitate to discern the two considered phenotypes (normoxia vs. hypoxia) in an unbiased manner. For this, we assigned the conditions to single cells by using the levels of the GFP marker at the threshold of log10 of 3 (with values above this threshold indicating the hypoxic condition). After assigning the conditions in this manner, we used the levels of unlabeled palmitate to classify the cells into the two phenotypes, achieving a classification accuracy of 87%. This accuracy validates the capacity of ^{13}C-SpaceM to identify the reduced contribution from glucose to palmitate through *de novo* fatty acid synthesis and thus determine the metabolic activity in a spatially-heterogeneous scenario at single-cell resolution.

^{13}C-SpaceM pseudo-bulk isotopologue profiles for palmitate match bulk results

As an additional step of validation, we compared the single-cell isotopologue profile as provided by ^{13}C-SpaceM with the bulk measurements. For bulk analysis, lipids were extracted from pooled cells individually for each condition using chloroform/methanol extraction [41], which allows the isolation of all major phospholipids as well as neutral lipids

and ceramides [37]. Lipid extracts were subjected to alkaline hydrolysis to release fatty acids and palmitate isotopologue distribution was determined by LC-MS.

This comparison showed an overall level of similarity, with pseudo-bulk intensities for the palmitate isotopologues detected by ^{13}C-SpaceM being reproduced by the bulk analysis in each condition (**Fig. 2e**). Importantly, the expected drastic changes induced upon hypoxia in the palmitate isotopologue distribution were reproduced in the bulk analysis: high fraction of unlabeled palmitate in hypoxia (> 0.9) as well as disappearance of isotopologues higher than M+2. However, there is a noticeable difference in the M+0 fraction detected in normoxic cells (average normalized intensity of 0.6 obtained by ^{13}C-SpaceM compared to 0.4 detected in the bulk analysis). One reason for this difference could be that the bulk data represent palmitate released through chemical hydrolysis from cellular lipids including neutral lipids. In contrast, the collision-induced dissociation of lipids used by ^{13}C-SpaceM is mostly specific to phospholipids and sphingolipids. Thus, the two methods interrogate palmitate from somewhat different lipid pools within the cell. In particular, triglycerides, which are included in the bulk method but excluded in the single-cell analysis due to it being restricted to the negative mode, could contribute a significant amount of newly synthesized fatty acids [42]. Consequently, our results imply that different lipid pools can incorporate newly synthesized fatty acids at different rates, thereby presenting different proportions of unlabeled molecules.

Summarizing the validation results obtained for the normoxia-hypoxia model, we conclude that ^{13}C-SpaceM can profile the contribution of glucose into *de novo* fatty acid synthesis and provide isotopologue distribution reflecting the labeling of palmitate as the key readout of the activity of this pathway, on the single-cell level.

Inducible ACLY knockdown reduces glucose contribution into *de novo* fatty acid synthesis

ACLY is a key enzyme of *de novo* fatty acid synthesis as it catalyzes the conversion of citrate into acetyl-CoA (**Fig. 1a**). We applied ^{13}C-SpaceM to investigate the effect of inducible ACLY knockdown on *de novo* fatty acid synthesis from glucose. We therefore

engineered cells to express short hairpin RNA sequences (shRNA) targeting murine *ACLY* under the control of a doxycycline-inducible promoter. The same promoter also drives expression of a GFP reporter, allowing identification of shRNA expressing cells. We used two non-overlapping shRNA sequences (ACLYkd oligo 1 and ACLYkd oligo 2) as well as a non-targeting control. Silencing was achieved by treating cells with 1 µg/ml of doxycycline for 72 hours, with both shRNA sequences resulting in a comparable level of ACLY depletion (**Fig. 3a**).

We next induced ACLY silencing in cells cultured in the presence of $^{13}C_6$-glucose and interrogated them with ^{13}C-SpaceM. Parallel cultures were analyzed using western blot (**Fig. 3b**) and bulk LC-MS-based stable isotope tracing. **Figure 3a** shows intensities of the isotopologues for palmitate released from cellular lipids for the cells expressing non-targeting shRNA and for cells with ACLYkd induced by either oligo 1 or oligo 2. For the control cells, the isotopologues M+10 and M+12 have maximal intensities in the bulk and single-cell analyses (**Fig. 3b**, left graphs). Pseudo-bulk analysis of ^{13}C-SpaceM data showing averages across all single cells indicates a higher M+0 fraction compared to the bulk analysis (normalized peak intensity of 0.6 compared to 0.3). This is in line with the results for the normoxia-hypoxia model in **Figure 2e** and, as discussed earlier, can be explained by differences in the specific lipid pools interrogated by the two methods. After ACLY silencing using oligo 1, we observed a marked shift in the isotopologue distribution with the intensities of isotopologues at M+2, M+4, and M+6 substantially increased (**Fig. 3a, middle graphs**). This is in line with our expectation that ACLY silencing reduces the contribution of glucose to the cytoplasmic acetyl-CoA pool. ACLY depletion using oligo 2 also induced a shift in the isotopologues distribution, with a peak between M+8 and M+10 (**Fig. 3a, right graphs**).

In contrast to the results obtained by comparing cells cultured under normoxic and hypoxic conditions, we could not discriminate the effect of knockdown (control vs. oligo 1 vs. oligo 2) based on the unlabeled palmitate ratio alone: the M+0 averages are similar between all three conditions (with the average values equal to 0.58, 0.52, and 0.62 for the control, oligo 1, and oligo 2 conditions, respectively). This can be explained by the

overall weaker effect of the induced ACLY knockdown compared to culturing under hypoxia. However, the intensities of isotopologues from M+2 to M+16 have visibly different distributions, showing higher intensities for isotopologues with lower mass upon knockdown when compared to control, clearly indicating a reduction in the glucose contribution to the cytoplasmic acetyl-CoA pool. Moreover, the impact of ACLY silencing on the overall contribution of *de novo* synthesis to the palmitate pool was more apparent in the bulk analysis (with M+0 fraction equal to 0.3, 0.37, and 0.43 for the control, oligo1, and oligo 2 conditions, respectively). This indicates that the lipid pool interrogated by ^{13}C-SpaceM is more dependent on fatty acid uptake.

Quantifying acetyl-CoA pool labeling degree for single cells

In **Figure 3a** we observed a pronounced shift towards a lower mass in the isotopologue distribution of palmitate upon the inducible knockdown of ACLY in both single-cell and bulk data. This shift indicates an increase of the fraction of unlabeled acetyl-CoA in the acetyl-CoA pool used for palmitate synthesis and is expected as ACLY catalyzes the production of cytoplasmic acetyl-CoA from citrate produced in its turn from labeled glucose [21]. We also noticed that ACLY silencing using shRNA oligo 1 resulted in a much wider distribution of isotopologues (cf. oligo 2) both in the bulk analysis and the pseudo-bulk display of the single-cell data. This is visible in **Figure 3a, middle graphs,** as higher intensities of the M+4 and in particular M+2 isotopologues for oligo 1 compared to oligo 2. The distribution of the pseudo-bulk (or bulk) intensities across the isotopologues for the oligo 1 data suggests the presence of two distinct populations with distinct responses to ACLY knockdown, with one population exhibiting a stronger effect of ACLY knockdown (with higher intensities at M+2 and M+4). We therefore used the power of single-cell analysis to deconvolve the relative palmitate labelling in individual cells from the three conditions (control, ACLYkd oligo 1 and ACLYkd oligo 2).

To analyze the single-cell heterogeneity of contribution from labeled ^{13}C-glucose into acetyl-CoA, for every cell we quantified the acetyl-CoA pool labeling degree as described in the methods. The estimated value *p* quantifies the ratio of labeled acetyl-CoA in the

cytosolic acetyl-CoA pool. This model can be applied to each single-cell profile of isotopic intensities of a fatty acid by estimating *p* that leads to best approximation of the data (the value *n* is known for a considered fatty acid, e.g. n=17 for palmitate). **Figure 3c** shows examples of such modeling for two cells, a control cell (grey) and an ACLYkd oligo 2 cell (blue). As expected, the ACLYkd cell demonstrates a lower acetyl-CoA pool labeling degree (*p* equal to 0.43 vs. 0.61).

Single-cell heterogeneity of flux from glucose to acetyl-CoA

Figure 3d shows results of quantifying the acetyl-CoA pool labeling degree (*p*) for single cells, plotted against the single-cell intensities of the GFP knockdown reporter. There is a clear difference between the control cells (grey) and cells with ACLY knockdown (ACLYkd oligo 1 in blue and ACLYkd oligo 2 in orange): as expected, an ACLY knockdown with either oligo 1 or oligo 2 leads to lower values of *p* (histogram peak in control at 0.6 compared to 0.35 in ACLYkd oligo1 and 0.4 in ACLYkd oligo 2).

Moreover, the differences between the two ACLYkd conditions (ACLYkd oligo 1 and ACLYkd oligo 2) are clearly visible. ACLY silencing using oligo 1 resulted in a bimodal distribution of the values of *p*, with a visibly higher variance (values ranging from 0.2 to 0.65). A bimodal distribution in single-cell results often indicates the presence of two subpopulations of cells. Notably, one mode of the distribution for the acetyl-CoA pool labeling degree in the ACLYkd oligo 1 condition displayed values for *p* in the range of 0.5-0.6 that overlaps with the acetyl-CoA pool labeling degree exhibited by the control cells (*p* of 0.5-0.7). This can be interpreted as the presence of a subpopulation of "weakly-silenced" cells where the ACLY knockdown was not sufficiently induced. This hypothesis is confirmed by the similarity of the GFP reporter data, where the GFP intensities for the ACLYkd oligo 1 cells also show a bimodal distribution. Indeed, ACLYkd oligo 1 cells with high values of *p* (above 0.5) also display GFP intensities similar to those of the WT cells (average log GFP intensity of 2.2 for the group with higher values of *p* and 2.6 for the group with lower *p*, compared to 1.9 for control). A possible explanation of the weak silencing in this subpopulation is that the silencing of ACLY did not work in these cells due to loss of the doxycycline-inducible expression cassette.

Interestingly, the second mode of the distribution of the acetyl-CoA pool labeling degree (*p*) for ACLYkd oligo 1 cells has a much lower value (0.35 cf. 0.55 for the first mode). This was clearly below the mode of the distribution of p for ACLYkd oligo 2 cells (equal to 0.42). This indicates the presence of a “strongly-silenced” subpopulation of ACLY oligo 1 cells in which silencing of ACLY was highly efficient, resulting in a strong reduction of acetyl-CoA labelling. Thus, we can interpret these results as the heterogeneity of ACLY knockdown using oligo 1 giving rise to two subpopulations of cells: “weakly-silenced” and “strongly-silenced” cells.

This is contrasted by the results for ACLY silencing using oligo 2. The acetyl-CoA pool labelling degree (*p*) as well as GFP reporter for these cells have values between “weakly-silenced” and “strongly-silenced” cells from the ACLYkd oligo 1 condition. Thus, one can interpret this data as ACLY knockdown using oligo 2 resulted in a more homogeneous cell population of “medium-silenced” cells.

Spatial information provided by ^{13}C-SpaceM offers another view at the cellular heterogeneity. **Figure 3e** shows ion images for three isotopic peaks of palmitate (M+0 in blue, M+2 in green, M+8 in red) for all three conditions (control, ACLYkd oligo 1 and ACLYkd oligo 2), with 3 replicates per condition. The M+2 peak was chosen as the most discriminative for the phenotype of low acetyl-CoA labelling that is specific to the “strongly-silenced” population among ACLYkd oligo 1 cells. The M+8 peak was chosen as a representative isotope for the control condition where fatty acids contain high numbers of ^{13}C. Thus, the difference between M+2 and M+8 as visible in **Fig. 3a** can serve as an indicator of the relative activity of the *de novo* fatty acid synthesis and thus be used to display heterogeneity. The data was acquired with the pixel size of 10 µm with cells having an average diameter of 550 µm, corresponding to 12 pixels per average cell. The ion images for ACLYkd oligo 1 showed a marked heterogeneity in the intensities of M+2 and M+8 isotopic peaks for palmitate that visualizes the presence of two distinct subpopulations in this condition: of “weakly-silenced” and “strongly-silenced” cells. Interestingly, we can see that these two subpopulations are spatially-heterogeneous that

rules out a batch effect or technical artifacts and indicates a single-cell effect. In contrast, ACLYkd oligo 2 cells show a more homogenous distribution of palmitate M+8 and an overall lower abundance of the palmitate M+2 isotopic peak to the degree that it's hardly visible in cells of ACLYkd oligo 2. The single-cell and spatial heterogeneity cannot be revealed through bulk analysis, demonstrating the unique advantages of the ^{13}C-SpaceM method.

^{13}C-SpaceM differentiates fatty acids by their relative uptake in single-cells

We next considered that ^{13}C-SpaceM data could be used to determine the relative uptake of different fatty acids as compared to their *de novo* synthesis (**Fig. 4b**). For each fatty acid, this was achieved by first performing natural isotope correction, normalizing all isotopologue peaks to the sum of all peaks, approximating isotopologues intensities with the binomial model described in the methods section, and taking the value of the "uptake" from the model. **Figure 4a** (upper plot) shows single-cell values of the relative uptake for the detected fatty acids: saturated fatty acids (SFAs) myristate, palmitate, stearate as well as mono-unsaturated fatty acids (MUFAs) palmitoleate and oleate, as determined in the control liver cancer cells. Interestingly, the levels of relative uptake at 60%-90% (and thus de novo synthesis of 10%-40%) are close to the reported rate of 30% of *de novo* lipogenesis in patients with NAFLD [43]. The two MUFAs, palmitoleate and oleate, showed a substantially higher relative uptake compared to the corresponding saturated fatty acids palmitate and stearate. This indicates that these cells mostly utilize uptake rather than *de novo* synthesis to obtain mono-unsaturated fatty acids. The results on the average levels were confirmed in the bulk LC-MS-based isotope tracing (**Fig. 4a**, lower plot).

We next employed the power of ^{13}C-SpaceM to investigate the relationships between the relative uptake of different fatty acids in the same cells. This was done by plotting and analyzing the single-cell values of relative uptake for each fatty acid vs. the others. This analysis showed no correlation of the relative uptake of myristate with any of the other fatty acids (**Fig. 4c, first column**). This lack of correlation is expected, as myristate was reported to be produced by *de novo* FA synthesis only to a small degree. Instead, myristate is mainly generated by the shortening of palmitate via peroxisomal β-oxidation

or the elongation of lauric acid [44]. In contrast, single-cell relative uptake values for palmitate, palmitoleate, stearate and oleate showed strong positive correlations (**Fig. 4c, columns 2-5**).

Overall, ^{13}C-SpaceM allowed to differentiate fatty acids by their sources specifically by exogenous uptake vs *de novo* synthesis. The lack of correlation for the single-cell uptake values for myristate likely reflects the specific mechanism of production or uptake of this fatty acid.

Effect of the induced ACLY knockdown on fatty acid uptake

Next, we investigated the effect of ACLY knockdown on fatty acid uptake. This analysis was restricted to ACLYkd using oligo 2 only, as the strong shift in the isotopologue distribution observed in upon ACLYkd using oligo 1 prohibited an accurate quantification of the fatty acid relative uptake (**see Fig. 3a, c**). Spatial analysis and visualization demonstrated a strong single-cell heterogeneity in the relative uptake of either palmitate or oleate in a mixed population of control and ACLYkd oligo 2 cells (**Fig. 4d and e**). More detailed and quantified analysis by plotting the single-cell relative uptake values separately for control and ACLYkd oligo 2 showed that ACLY-silenced cells increased the uptake of palmitate (histogram peak at 0.55 in control compared to 0.61 in ACLYkd), with each population displaying a unimodal symmetric distribution (**Fig. 4f**). Oleate uptake, which was already higher compared to palmitate uptake in the control cells, was also increased after ACLY knockdown (histogram peak at 0.85 in control compared to 0.95 in ACLYkd). In addition, we observed an asymmetric (skewed) unimodal distribution of the oleate single-cell relative uptake values for the ACLYkd population, with more cells showing high relative uptake values. This indicates that some cells of the population respond to ACLY silencing by selectively inducing the uptake of mono-unsaturated fatty acids, such as oleate.

Taken together, we have presented ^{13}C-SpaceM, a novel method for spatial single-cell isotope tracing, and demonstrated how it can help interrogate the activity of *de novo* fatty acid synthesis. The key novelty of the method compared to the previously published

method SpaceM for spatial single-cell metabolomics is in using All-Ion-Fragmentation combined with fatty acid isotopologues analysis and modeling. ^{13}C-SpaceM can provide detailed insights into the heterogeneity of *de novo* fatty acid synthesis in cancer cells by quantifying single-cell heterogeneity of acetyl-CoA metabolism and fatty acid uptake in phenotypically distinct cell populations. Concluding, ^{13}C-SpaceM addresses the need to investigate the activity of well-characterized metabolic pathways on the single-cell level. ^{13}C-SpaceM can dissect single-cell metabolic heterogeneity as well as reveal subpopulations of cells which differ in their metabolic state yet are hidden from the bulk analyses.

Discussion

The advance of single-cell omics technologies has revolutionized insight into the genetic and phenotypic heterogeneity of cell populations at the levels of tissues, organs and whole organisms [26]. This is of particular importance in cancer research, as tumors consist of multiple subclones of cancer cells as well as a highly diverse population of stromal cells, both of which are exposed to microenvironmental conditions that can change profoundly in a spatial and temporal manner [45]. Complementing the paradigm of genetic heterogeneity of cancer cells [46] [47], there is an emerging acknowledgment of the heterogeneity of metabolic states of cancer cells. Determined by genetic and epigenetic alterations, their metabolic states are influenced by non-genetic factors such as the tissue of origin, nutrients and oxygen availability in the microenvironment as well as local interactions with the tumor stroma and immune cells [48]. Single-cell transcriptomics has provided insights into co-existence of distinct metabolic states in populations of cancer cells, such as a shift towards mitochondrial oxidative phosphorylation observed in micrometastases compared to primary tumor in breast cancer [49]. Recent technological advances in mass spectrometry, including electrospray ionization (ESI), matrix-assisted laser desorption/ionization (MALDI) or dielectric barrier discharge ionization (DBDI) in combination with advanced computational methods enabled detecting profiles of polar metabolites and lipids from single cells [30, 31, 50]. While these methods have provided unprecedented insight into the metabolic states of single cells, they fail to capture the dynamic activity of metabolic processes and the degree of flexibility within the metabolic

network. At the same time, stable-isotope tracing has emerged as the gold-standard to reveal metabolic activity in cells and tissues in bulk [51] and in spatially-resolved manner [52], yet was not demonstrated so far in single cells.

We developed ^{13}C-SpaceM, a method to combine stable-isotope tracing with spatial single-cell metabolomics to determine *de novo* fatty acid biosynthesis in cancer cells at single-cell resolution. ^{13}C-SpaceM builds upon SpaceM [31] with the major changes including the mass spectrometry method constructed to mimic chemical saponification and fatty acid detection as in bulk stable isotope tracing as well as the data analysis. In particular, we demonstrate how using the binomial model applied to the isotopologue distribution helps estimate such labeling parameters as uptake and pool labeling degree for individual cells.

^{13}C-SpaceM as employed in this study uses all-ion fragmentation to release fatty acids from cellular lipids at m/z range of 600-1000 and ionized in the negative mode, thereby focusing on glycerophospholipids and sphingolipids while mostly excluding lysophospholipids, triglycerides and cardiolipins [37]. This selectivity in mass range can be used to selectively monitor labelling in fatty acids present in specific lipid classes, in this case in the lipids most abundant in cell membranes. Indeed, when comparing ^{13}C-SpaceM data to bulk stable isotope tracing in fatty acids after saponification of total cellular lipids from the same cells, we noticed a larger proportion of palmitate derived from *de novo* synthesis in the bulk analysis. As the cells used in this study have already reached isotopic steady state after 72 hours in the presence of ^{13}C-glucose, this result suggests that the synthesis of specific lipids utilizes distinct pools of palmitate that differ in their contribution from *de novo* fatty acid synthesis and uptake [6]. Local fatty acid channeling into phospholipid synthesis has been observed during the rapid formation of the autophagic membrane in yeast [53], indicating that lipid synthesis can take place in a context-specific manner.

We validated the ability of ^{13}C-SpaceM to detect changes in glucose-dependent fatty acid synthesis, and its single-cell resolution, by co-plating cells that had previously been cultured under either normoxia or hypoxia. This system was chosen as hypoxia leads to a global reprogramming of cellular lipid metabolism [10]. Spatial single-cell isotope tracing by ^{13}C-SpaceM was able to clearly separate the two cell populations based on the strong

increase in the M+0 fraction of palmitate observed in hypoxic cells. This is expected, as hypoxia reduces the conversion of glucose-derived pyruvate into mitochondrial acetyl-CoA via induction of pyruvate dehydrogenase kinase 1 (PDK1) [54], thereby lowering the flux of glucose carbons into the TCA cycle and subsequently into the lipogenic (cytoplasmic) acetyl-CoA pool. At the same time, hypoxia induces the reductive carboxylation of glutamine thus generating cytoplasmic citrate to support lipid synthesis [19, 20] and the direct synthesis of acetyl-CoA from acetate [21, 22]. In addition, hypoxia leads to the uptake of exogenous fatty acids [18, 39], further increasing the proportion of the M+0 fraction.

We also assessed the application of ^{13}C-SpaceM to monitor the effect of perturbations of the metabolic network in cancer cells. Both bulk and single-cell analysis revealed a marked shift in palmitate isotopologue distribution following silencing of ACLY, correctly reflecting a reduced contribution of ^{13}C-glucose to the lipogenic acetyl-CoA pool. Using a binomial model to quantify fractional labelling from the isotopologue distribution [21], we estimated the labelling degree of acetyl-CoA in control and ACLY silenced cells at single-cell level. In agreement with previous studies using bulk analysis of palmitate isotopologue distribution in ACLY wildtype vs knockout mouse embryo fibroblasts [24], silencing ACLY caused a reduction in the fractional labelling of acetyl-CoA from glucose but only a minor increase in the M+0 fraction. This suggests that other substrates, such as acetate, are used to synthesize acetyl-CoA under these conditions [24]. Our analysis also revealed a substantial degree of heterogeneity in fractional labelling of lipogenic acetyl-CoA within the cell population, particularly after silencing ACLY. This heterogeneity suggested differences in the silencing efficiency of the different oligonucleotides used to target ACLY, which were completely obscured in the bulk analysis. Acetyl-CoA plays a central role in the metabolism of cancer cells, as it is not only used as a substrate for fatty acid and cholesterol synthesis but is also essential for post-translational modification of proteins, most importantly histones. Methods to quantify acetyl-CoA synthesis from different substrates at single-cell level can reveal the link between metabolism and genetic or environmental factors.

We also used ^{13}C-SpaceM to determine the relative proportion of *de novo* synthesis and uptake of five non-essential fatty acids at single-cell level. While fatty acids can be taken

up by cells through passive diffusion, it is generally concluded that uptake functions through receptor-mediated processes [55]. Moreover, fatty acid uptake via the scavenging receptor CD36 has been shown to facilitate metastasis formation by promoting a stem cell phenotype in cancer [56]. Our single-cell analysis revealed substantial heterogeneity in relative uptake for the different fatty acid within the population of cancer cells. Moreover, correlation analysis indicated increased uptake of palmitoleate and oleate, suggesting a higher demand for mono-unsaturated fatty acids. ACLY silencing resulted in a general increase in fatty acid uptake, in particular palmitate and oleate, indicating that limiting the conversion of citrate to acetyl-CoA lowers the ability of cancer cells to fulfil their fatty acid demand via de novo synthesis [24].

Interestingly, a recent single-cell lipidomics study investigated the effect of chemical inhibition of ACLY on intracellular lipids in pancreatic cancer cells [30]. Their findings revealed a reduction of specific PC species containing saturated and mono-unsaturated fatty acids upon ACLY inhibition. This is consistent with our observations, as a reduction in *de novo* fatty acid synthesis would selectively reduce the availability of saturated and mono-unsaturated fatty acids for lipid synthesis und could therefore explain the reduction in these lipid species.

Together, the results presented here present ^{13}C-SpaceM as a method for spatial single-cell isotope tracing able to monitor *de novo* fatty acid synthesis, production of lipogenic acetyl-CoA and fatty acid uptake of heterogenous cell populations exposed to genetic and environmental perturbations. Through additional modifications of this approach, for example by applying different metabolic tracers or by restricting collision-induced dissociation to individual lipid classes, ^{13}C-SpaceM can provide broader or more specific information about activity of the *de novo* lipid biogenesis at the single-cell resolution. Furthermore, by detecting other metabolite classes with the underlying MALDI-imaging mass spectrometry as already demonstrated [52], ^{13}C-SpaceM can be extended for stable isotope tracing of other metabolic pathways thus opening avenues towards revealing and understanding single-cell heterogeneity of metabolic activity.

References

1. Harayama, T. & Riezman, H. Understanding the diversity of membrane lipid composition. *Nat Rev Mol Cell Biol* **19**, 281-296 (2018).
2. Farese, R.V., Jr. & Walther, T.C. Lipid droplets finally get a little R-E-S-P-E-C-T. *Cell* **139**, 855-860 (2009).
3. Wang, D. & Dubois, R.N. Eicosanoids and cancer. *Nat Rev Cancer* **10**, 181-193 (2010).
4. Park, J.B. *et al.* Phospholipase signalling networks in cancer. *Nat Rev Cancer* **12**, 782-792 (2012).
5. Vanhaesebroeck, B., Stephens, L. & Hawkins, P. PI3K signalling: the path to discovery and understanding. *Nat Rev Mol Cell Biol* **13**, 195-203 (2012).
6. Currie, E., Schulze, A., Zechner, R., Walther, T.C. & Farese, R.V., Jr. Cellular fatty acid metabolism and cancer. *Cell Metab* **18**, 153-161 (2013).
7. Rohrig, F. & Schulze, A. The multifaceted roles of fatty acid synthesis in cancer. *Nat Rev Cancer* **16**, 732-749 (2016).
8. Snaebjornsson, M.T., Janaki-Raman, S. & Schulze, A. Greasing the Wheels of the Cancer Machine: The Role of Lipid Metabolism in Cancer. *Cell Metab* **31**, 62-76 (2020).
9. Koundouros, N. & Poulogiannis, G. Reprogramming of fatty acid metabolism in cancer. *Br J Cancer* **122**, 4-22 (2020).
10. Munir, R., Lisec, J., Swinnen, J.V. & Zaidi, N. Lipid metabolism in cancer cells under metabolic stress. *Br J Cancer* **120**, 1090-1098 (2019).
11. Peck, B. & Schulze, A. Lipid desaturation - the next step in targeting lipogenesis in cancer? *FEBS J* **283**, 2767-2778 (2016).
12. Griffiths, B. *et al.* Sterol regulatory element binding protein-dependent regulation of lipid synthesis supports cell survival and tumor growth. *Cancer & metabolism* **1**, 3 (2013).
13. Young, R.M. *et al.* Dysregulated mTORC1 renders cells critically dependent on desaturated lipids for survival under tumor-like stress. *Genes & development* **27**, 1115-1131 (2013).
14. Williams, K.J. *et al.* An essential requirement for the SCAP/SREBP signaling axis to protect cancer cells from lipotoxicity. *Cancer research* (2013).
15. Rudalska, R. *et al.* LXRα activation and Raf inhibition trigger lethal lipotoxicity in liver cancer. *Nature Cancer* **2**, 201-217 (2021).
16. Peck, B. *et al.* Inhibition of fatty acid desaturation is detrimental to cancer cell survival in metabolically compromised environments. *Cancer & metabolism* **4**, 6 (2016).
17. Magtanong, L. *et al.* Exogenous Monounsaturated Fatty Acids Promote a Ferroptosis-Resistant Cell State. *Cell Chem Biol* **26**, 420-432 e429 (2019).
18. Kamphorst, J.J. *et al.* Hypoxic and Ras-transformed cells support growth by scavenging unsaturated fatty acids from lysophospholipids. *Proceedings of the National Academy of Sciences of the United States of America* **110**, 8882-8887 (2013).
19. Metallo, C.M. *et al.* Reductive glutamine metabolism by IDH1 mediates lipogenesis under hypoxia. *Nature* **481**, 380-384 (2011).
20. Wise, D.R. *et al.* Hypoxia promotes isocitrate dehydrogenase-dependent carboxylation of alpha-ketoglutarate to citrate to support cell growth and viability. *Proc Natl Acad Sci U S A* **108**, 19611-19616 (2011).
21. Kamphorst, J.J., Chung, M.K., Fan, J. & Rabinowitz, J.D. Quantitative analysis of acetyl-CoA production in hypoxic cancer cells reveals substantial contribution from acetate. *Cancer & metabolism* **2**, 23 (2014).
22. Schug, Z.T. *et al.* Acetyl-CoA synthetase 2 promotes acetate utilization and maintains cancer cell growth under metabolic stress. *Cancer cell* **27**, 57-71 (2015).
23. Sivanand, S., Viney, I. & Wellen, K.E. Spatiotemporal Control of Acetyl-CoA Metabolism in Chromatin Regulation. *Trends Biochem Sci* **43**, 61-74 (2018).

24. Zhao, S. *et al.* ATP-Citrate Lyase Controls a Glucose-to-Acetate Metabolic Switch. *Cell reports* **17**, 1037-1052 (2016).
25. Bulusu, V. *et al.* Acetate Recapturing by Nuclear Acetyl-CoA Synthetase 2 Prevents Loss of Histone Acetylation during Oxygen and Serum Limitation. *Cell reports* **18**, 647-658 (2017).
26. Heath, J.R., Ribas, A. & Mischel, P.S. Single-cell analysis tools for drug discovery and development. *Nat Rev Drug Discov* **15**, 204-216 (2016).
27. Duncan, K.D., Fyrestam, J. & Lanekoff, I. Advances in mass spectrometry based single-cell metabolomics. *Analyst* **144**, 782-793 (2019).
28. Ellis, J.M. & Wolfgang, M.J. A genetically encoded metabolite sensor for malonyl-CoA. *Chem Biol* **19**, 1333-1339 (2012).
29. Guo, Z. *et al.* Single-Cell Profiling of Fatty Acid Uptake Using Surface-Immobilized Dendrimers. *J Am Chem Soc* **143**, 11191-11198 (2021).
30. Liu, Q. *et al.* High-Throughput Single-Cell Mass Spectrometry Reveals Abnormal Lipid Metabolism in Pancreatic Ductal Adenocarcinoma. *Angew Chem Int Ed Engl* **60**, 24534-24542 (2021).
31. Rappez, L. *et al.* SpaceM reveals metabolic states of single cells. *Nat Methods* **18**, 799-805 (2021).
32. Tumanov, S., Bulusu, V. & Kamphorst, J.J. Analysis of Fatty Acid Metabolism Using Stable Isotope Tracers and Mass Spectrometry. *Methods Enzymol* **561**, 197-217 (2015).
33. Heinrich, P. *et al.* Correcting for natural isotope abundance and tracer impurity in MS-, MS/MS- and high-resolution-multiple-tracer-data from stable isotope labeling experiments with IsoCorrectoR. *Sci Rep* **8**, 17910 (2018).
34. Stringer, C., Wang, T., Michaelos, M. & Pachitariu, M. Cellpose: a generalist algorithm for cellular segmentation. *Nat Methods* **18**, 100-106 (2021).
35. Millard, P. *et al.* IsoCor: isotope correction for high-resolution MS labeling experiments. *Bioinformatics* **35**, 4484-4487 (2019).
36. Wolf, F.A., Angerer, P. & Theis, F.J. SCANPY: large-scale single-cell gene expression data analysis. *Genome Biol* **19**, 15 (2018).
37. Tumanov, S. & Kamphorst, J.J. Recent advances in expanding the coverage of the lipidome. *Curr Opin Biotechnol* **43**, 127-133 (2017).
38. Mullen, A.R. *et al.* Reductive carboxylation supports growth in tumour cells with defective mitochondria. *Nature* **481**, 385-388 (2012).
39. Bensaad, K. *et al.* Fatty acid uptake and lipid storage induced by HIF-1alpha contribute to cell growth and survival after hypoxia-reoxygenation. *Cell reports* **9**, 349-365 (2014).
40. Scaglia, N., Tyekucheva, S., Zadra, G., Photopoulos, C. & Loda, M. De novo fatty acid synthesis at the mitotic exit is required to complete cellular division. *Cell Cycle* **13**, 859-868 (2014).
41. Bligh, E.G. & Dyer, W.J. A rapid method of total lipid extraction and purification. *Can J Biochem Physiol* **37**, 911-917 (1959).
42. Ackerman, D. *et al.* Triglycerides Promote Lipid Homeostasis during Hypoxic Stress by Balancing Fatty Acid Saturation. *Cell reports* **24**, 2596-2605 e2595 (2018).
43. Donnelly, K.L. *et al.* Sources of fatty acids stored in liver and secreted via lipoproteins in patients with nonalcoholic fatty liver disease. *J Clin Invest* **115**, 1343-1351 (2005).
44. Rioux, V., Catheline, D. & Legrand, P. In rat hepatocytes, myristic acid occurs through lipogenesis, palmitic acid shortening and lauric acid elongation. *Animal* **1**, 820-826 (2007).
45. Li, Z., Seehawer, M. & Polyak, K. Untangling the web of intratumour heterogeneity. *Nat Cell Biol* **24**, 1192-1201 (2022).
46. Hausser, J. & Alon, U. Tumour heterogeneity and the evolutionary trade-offs of cancer. *Nat Rev Cancer* **20**, 247-257 (2020).

47. Kim, C. *et al.* Chemoresistance Evolution in Triple-Negative Breast Cancer Delineated by Single-Cell Sequencing. *Cell* **173**, 879-893 e813 (2018).
48. Kim, J. & DeBerardinis, R.J. Mechanisms and Implications of Metabolic Heterogeneity in Cancer. *Cell Metab* **30**, 434-446 (2019).
49. Davis, R.T. *et al.* Transcriptional diversity and bioenergetic shift in human breast cancer metastasis revealed by single-cell RNA sequencing. *Nat Cell Biol* **22**, 310-320 (2020).
50. Fujii, T. *et al.* Direct metabolomics for plant cells by live single-cell mass spectrometry. *Nat Protoc* **10**, 1445-1456 (2015).
51. Jang, C., Chen, L. & Rabinowitz, J.D. Metabolomics and Isotope Tracing. *Cell* **173**, 822-837 (2018).
52. Wang, L. *et al.* Spatially resolved isotope tracing reveals tissue metabolic activity. *Nat Methods* **19**, 223-230 (2022).
53. Schutter, M., Giavalisco, P., Brodesser, S. & Graef, M. Local Fatty Acid Channeling into Phospholipid Synthesis Drives Phagophore Expansion during Autophagy. *Cell* **180**, 135-149 e114 (2020).
54. Kim, J.W., Tchernyshyov, I., Semenza, G.L. & Dang, C.V. HIF-1-mediated expression of pyruvate dehydrogenase kinase: A metabolic switch required for cellular adaptation to hypoxia. *Cell Metab* **3**, 177-185 (2006).
55. Samovski, D., Jacome-Sosa, M. & Abumrad, N.A. Fatty Acid Transport and Signaling: Mechanisms and Physiological Implications. *Annu Rev Physiol* (2022).
56. Pascual, G. *et al.* Targeting metastasis-initiating cells through the fatty acid receptor CD36. *Nature* **541**, 41-45 (2017).

Figures

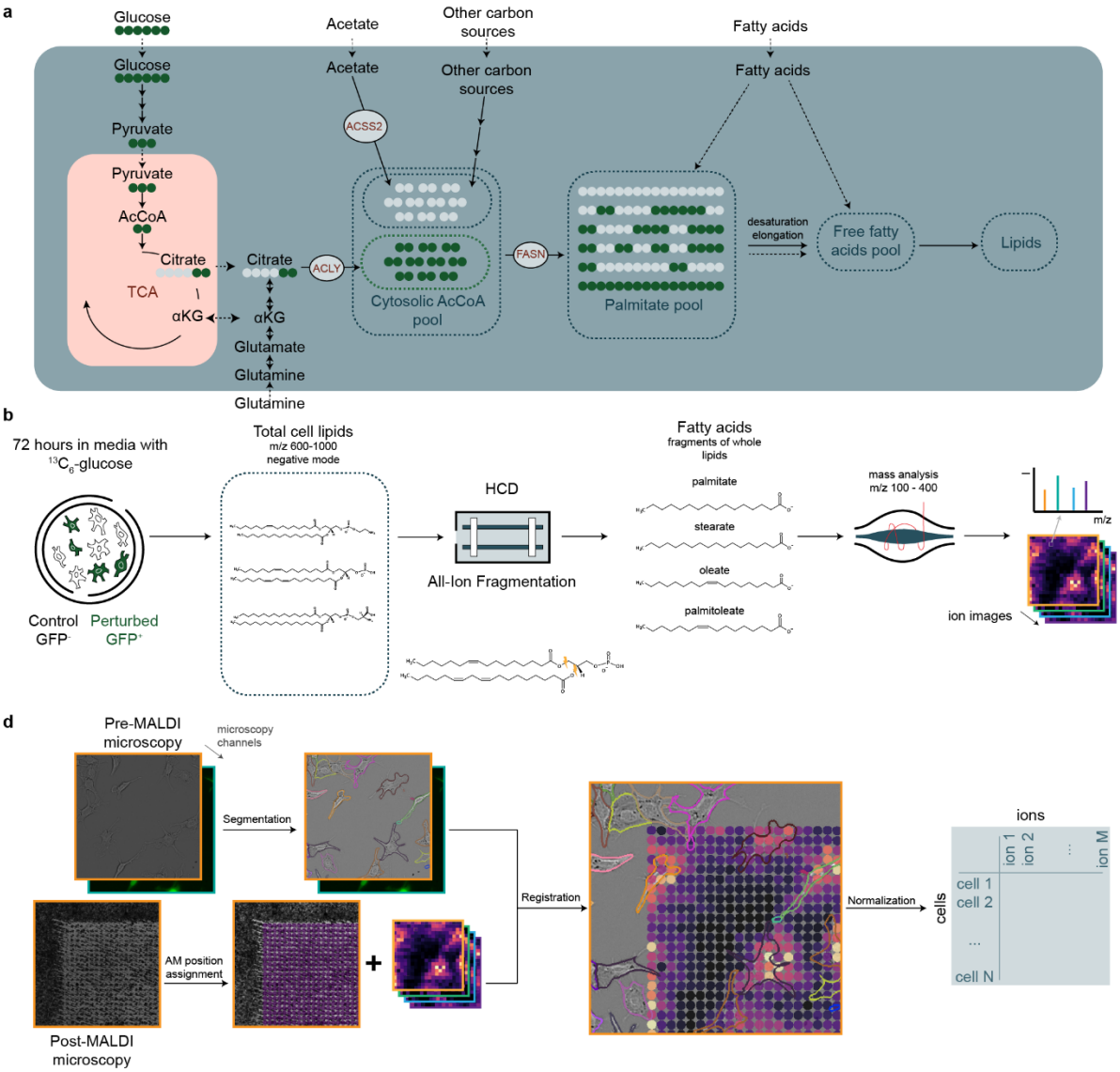

Figure 1. ^{13}C-SpaceM workflow as applied to interrogate *de novo* fatty acid synthesis

a) Generation of cytoplasmic acetyl-CoA and subsequent fatty acid and lipid synthesis from stable-isotope labelled $^{13}C_6$-glucose. Glucose-derived pyruvate is metabolized in the mitochondria and exported to the cytoplasm in the form of citrate. ATP-citrate lyase (ACLY) converts citrate to acetyl-CoA, thereby contributing to the cytoplasmic (lipogenic) acetyl-CoA pool. *De novo* fatty acid synthesis by fatty acid synthase (FASN) results in the formation of palmitate (C16:0), which is either further modified or directly incorporated into cellular lipids. Exogenously taken up fatty acids are also incorporated into cellular lipids but are not labelled.

b) Using all-ion fragmentation imaging mass spectrometry for ^{13}C-SpaceM. Cells are grown in medium supplemented with uniformly labelled $^{13}C_6$-glucose for 72 hours. The combination of wide-range isolation of parent lipid ions followed by HCD fragmentation and selective isolation of fatty acid fragments allows high-sensitivity measurements of fatty acids incorporated into lipids,

conceptually similar to bulk extractions followed by saponification but with the benefit of retained spatial information and the exclusion of free fatty acids.

c) Integration of microscopy and imaging mass spectrometry in ^{13}C-SpaceM to obtain single-cell profiles. Pre-MALDI microscopy and post-MALDI microscopy images containing information about the cell outlines and areas ablated by MALDI-imaging are registered. Ion intensities from MALDI-imaging are assigned to single cells through a normalization procedure.

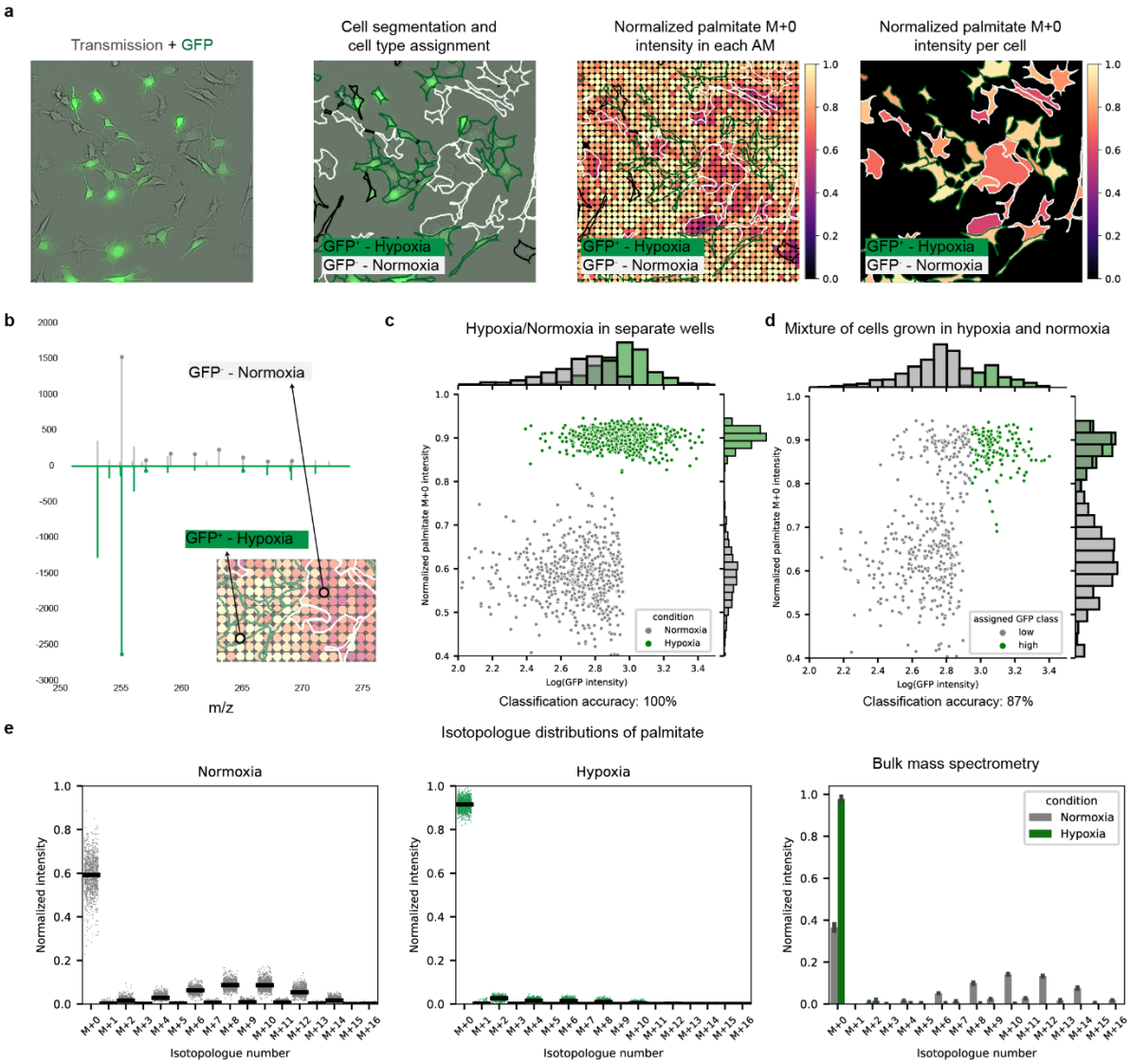

Figure 2. Validating ^{13}C-SpaceM by interrogating *de novo* fatty acid synthesis in spatially-heterogeneous normoxia-hypoxia model

a) Illustration of microscopy and imaging mass spectrometry data from the model of co-plated primary murine liver cancer cells originally cultured under normoxia (GFP-negative) and hypoxia (GFP-positive). The GFP signal was used for discerning the culturing conditions (white and green cell outlines shown normoxic and hypoxic cells, respectively). The normalized intensities of the M+0 isotope of palmitate (representing the fraction of unlabelled palmitate) are shown for MALDI-imaging pixels and as assigned to the single cells.

b) Mass spectra for individual pixels mapped to cells from a normoxic cell (white outline) and a hypoxic cell (green outline). The peaks corresponding to palmitate isotopologues are marked by grey or green dots.

c and d) Discerning cells cultured under normoxia vs. hypoxia using ^{13}C-SpaceM for the cells mono-plated for each culturing condition (C) and for spatially-heterogeneous co-plated cells from both conditions (D). Scatterplot shows the values of the GFP-reporter (ground truth for telling the

condition) and the normalized intensity of the M+0 isotope of palmitate representing the fraction of unlabelled palmitate for single cells.

e) Comparison of single-cell vs. bulk intensities for the M+0 isotope of palmitate. Single-cell intensities are from the spatially-heterogeneous co-plated model. Bulk intensities are from cells of each mono-cultured condition subjected to total fatty acid analysis by saponification followed by LC-MS/MS. For single-cell data, black lines show average values. For bulk data, data are displayed as mean ± standard deviation across 3 replicates.

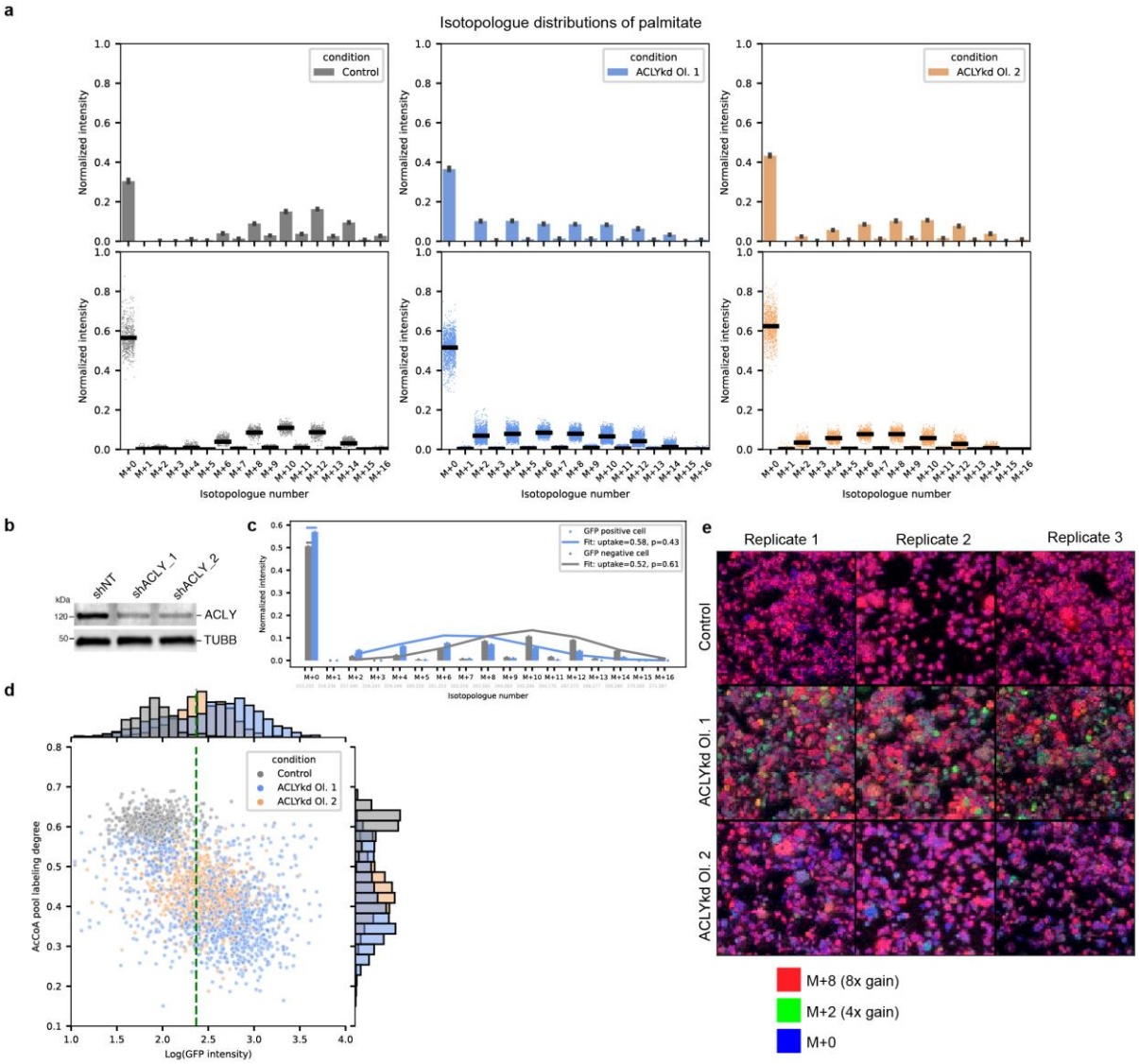

Figure 3. Single-cell quantitative analysis of lipogenic acetyl-CoA production and heterogeneity

a) Comparison of bulk and single-cell analysis of isotopologue distribution for palmitate after 72 hours of ACLY gene silencing and culture in the presence of $^{13}C_6$-glucose. Bulk data are displayed as mean ± standard deviation across 3 replicates. For single-cell data, black lines show average values.

b) Immunoblot of protein lysates showing efficiency of ACLY knockdown using two shRNA sequences (ACLYkd oligo1 and ACLYkd oligo 2) compared to non-targeting control (shNT). Tubulin B (TUBB) is shown as loading control.

c) Normalized single-cell isotopologues distribution for two individual cells, one from the control and the other from ACLYkd oligo 1 (shown as bar plots). Lines show fit of the fatty acid labelling binomial model: horizontal lines for M+0 showing an estimated uptake, and connected lines for

M+2i showing (1 - uptake) * binomial(i). Legend shows parameters of the binomial model fit.
d) Single-cell analysis of the estimated acetyl-CoA pool labelling degree (*p*) as calculated using the fatty acid labelling binominal model for the three conditions: control (grey), ACLYkd oligo 1 (blue), and ACLYkd oligo 2 (blue). Green dashed line shows 95% quantile of the GFP intensity distribution in the control condition, which was used to classify cells as GFP-positive vs. GFP-negative.
e) Spatial metabolic imaging of *de novo* fatty synthesis for the control, ACLYkd oligo 1, and ACLYkd oligo 2 conditions. Abundance of different palmitate isotopic peaks are displayed in different channels: M+0 (blue), M+2 (green) and M+8 (red). Each channel is normalized to the total ion count (TIC).

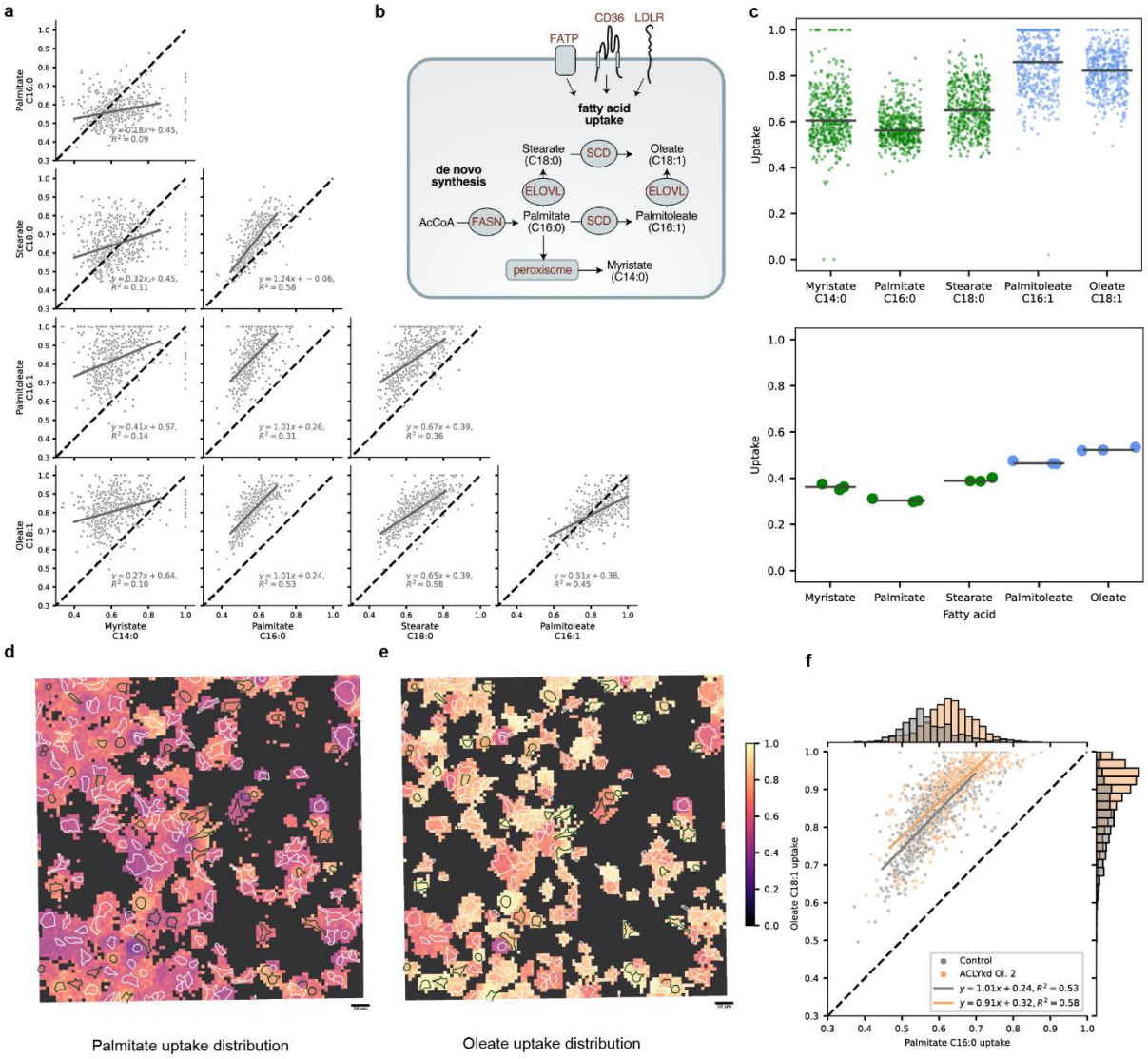

Figure 4. ^{13}C-SpaceM differentiates fatty acids by their relative uptake in single-cells

a) Correlation of uptake of different fatty acids. Dashed line is the diagonal. For each pair of fatty acids, the linear fit is shown as a grey line, with the fit parameters shown in the legend.

Schematic of biosynthesis of different fatty acids?

b) Diagram showing mechanisms involved in fatty acid synthesis, desaturation and uptake.

c) Fatty acids uptake in the control cells as determined for myristate, palmitate, palmitoleate, stearate and oleate; saturated fatty acids in green and unsaturated fatty acids in blue. Top: Single-cell data with each point representing a cell, black horizontal lines showing median values. Bottom: Data from the bulk stable isotope tracing.

d and e) Spatial metabolic imaging of the fatty acid uptake in co-plated cells from two conditions (control and ACLYkd oligo 2). Each square corresponds to one MALDI pixel. Pixels with the total intensity of the fatty acid isotopes below the set limit of detection (1000) are shown in black. Cell outlines are green for GFP-positive cells and white for GFP-negative cells. Pixels are colored

according to the normalized M+0 describing the uptake contribution for a given fatty acid. D: Normalized M+0 of palmitate. E: Normalized M+0 of oleate.

f) Single-cell analysis of how fatty acid uptake changes upon ACLY knockdown. Dashed line is the diagonal. For each condition the linear fit is shown in the corresponding color, with the fit parameters shown in the legend.